The STAMAS Simulator: A Kinematics and Dynamics Simulator for an Astronaut's Leg and Hand Exoskeleton

Ricardo González Camarero, Thomas Hulin, Bernhard Vodermayer

***Abstract*— In the scope of the European project STAMAS, novel exoskeleton based exercise and support devices for an astronaut's leg and hand are developed. The STAMAS simulator is capable of simulating the dynamic interaction between the astronaut and these two exoskeleton prototypes. It comprises components for the calculation of the kinematics and dynamics of the device and the astronaut's extremities, as well as a virtual reality viewer for visualization. The simulator not only offers efficient and inexpensive access to the behavior of the systems, but also is a veritable key element towards the assessment of the safety for the astronaut, for the equipment and for the mission. Simulations that have been conducted could confirm the concepts of both exoskeletons and reveal the mechanical strain and the required actuator forces.**

I. Introduction

The research project STAMAS (Smart Technology for Artificial Muscle Applications in Space) targets at developing new types of astronauts' exoskeletons for the leg and for the hand. Two demonstrators will be integrated to tackle two vital and challenging problems of manned space flight, i.e., chronic physiological degradation due to the effect of microgravity, and hand fatigue during extravehicular activities (EVAs) caused by high resistance forces inside a space suit. The leg device has the function as a countermeasure device, while the hand exoskeleton aims at supporting astronauts during EVAs.

The exoskeletons are driven by shape memory alloy (SMA) actuators and, for the leg, additionally by electroactive polymers (EAP). Due to challenging limitation with regard to weight and available space that arise from the application space, these actuators promise to be advantageous compared to electric motors, as they offer high power density at small installation space.

The present paper describes the dynamic and kinematic simulator that has been developed in the STAMAS project. For both planned demonstrators, a simulator was developed that takes into account the different properties of the two devices and of the different limbs. The simulator has the three main goals:

The research was funded by the STAMAS Project of the EU Seventh Framework Programme FP7/2007-2013 under Grant 312815 STAMAS.

The presented work was partially conducted in the scope of the diploma thesis of Ricardo González Camarero.

The authors are with the Institute of Robotics and Mechatronics, DLR (German Aerospace Center), D-82234 Wessling, Germany. Thomas.Hulin@dlr.de

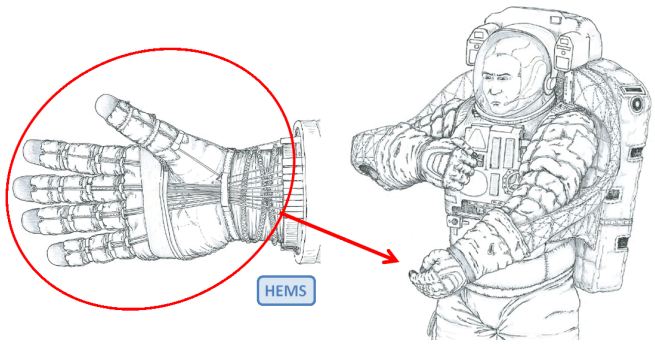

Fig. 1. Concept drawing of the STAMAS hand exoskeleton, also named Hand Exo-Muscular System (HEMS) [1]. Tendons are pulling at the finger tips to support the astronaut closing her/his hand during EVAs.

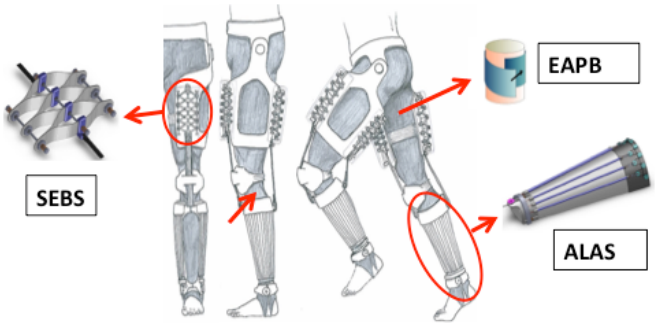

Fig. 2. Concept drawing of the STAMAS leg exoskeleton with its three main components, i.e., a Smart Elastic Bands System (SEBS), an Ankle Lateral Actuation System (ALAS), and Electro-Active Polymers Bands (EAPB) [1].

1) Evaluate the suitability of the demonstrator concepts to generate the required movements for the two target applications, i.e., countermeasure training and supporting the astronaut to close hands.
2) Determine the required actuator forces for each targeted application.
3) Provide a testing environment for the STAMAS controllers, so that they can be tested in simulation prior to integrating them onto the hardware prototypes.

To meet these goals, particular attention was paid to realistic kinematics and dynamics of an astronaut hand and leg during the development of the simulator. As far as it was possible, the link lengths and masses of the limbs were chosen according to the NASA standards (chapter on "Anthropometry and Biomechanics" in Volume I of the Man-Systems Integration Standards [2]). The simulator does not only contain a dynamics and kinematic module but, in addi-

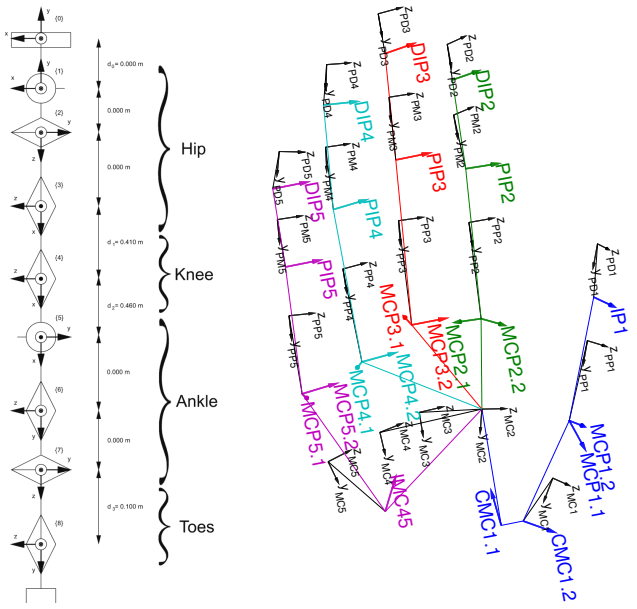

(a) leg kinematics (b) hand kinematics

Fig. 3. The kinematic schematics for the leg and the right human hand. Rotations occur around the z-axis. For the hand, the colored axes indicate the rotation axis of each joint.

tion, it provides an expert GUI and a virtual reality viewer that in combination enable comprehensive parameterization of and interaction with the simulation.

The simulator represents a key element towards safety for the astronaut, for the equipment, and for the mission because – by meeting above goals – it allows for intense simulative testing of the STAMAS controllers and the device sketches. This document is structured as follows. Section II describes the human kinematic and dynamic model that was assumed in the simulator. Section III presents the key modules of the STAMAS simulator. Section IV provides simulation results. Section V concludes this document. The appendix contains a concise state of the art review on human exoskeleton simulations.

II. Human Kinematic and Dynamic Model

This section presents the kinematic and dynamic models for the hand and the leg that are used for the simulator. The Denavit-Hartenberg (DH) convention [3] is used as mathematical basis to describe the kinematic chains. This method is widely applied in the field of robotics and may be found in numerous text books, e.g., Asada and Slotine [4], or Craig [5]. It has the advantage of requiring only four parameters per joint compared to other transformation representations. The movements of rotations of the revolute joints occur around the z-axis.

The dynamics computation is based on the dynamics equation of motion [5],

$$\tau + \tau_{\text{ext}} = M(q)\,\ddot{q} + C(q,\dot{q})\,\dot{q} + g(q), \qquad (1)$$

with joint angles q, the applied and external torques τ and τ_{ext}, the mass matrix M, the centrifugal, Coriolis and friction matrix C, and the gravity vector g, which vanishes in microgravity applications. The mass matrix M is calculated using the recursive Newton-Euler formulation [5]. The algorithm to perform this calculation was parameterized with the corresponding values given in the following sub-sections.

TABLE I

The DH-parameters of the leg model.

α/(degrees)	a/(m)	θ/(degrees)	d/(m)
0	0	0	0
90	0	90	0
90	0	90	0
0	0.393	0	0
−90	0.363	0	0
90	0	−90	0
−90	0	0	0
90	−0.15	0	0

A. Leg

The leg is modeled as a serially kinematic chain with eight revolute joints (see Fig. 3(a)). It has three degrees of freedom (DoF) for the hip joint, one for the knee, three for the ankle, and one for the toes. This configuration was chosen to allow for walking simulations on countermeasure devices for space applications, such as the COLBERT [6].

Link lengths, masses, moments of inertia, joint motion ranges and centers of gravity were defined using the NASA standards [2] and other related work [7], [8], [9]. The values used for the leg model are shown in Table I and Table II. To determine the movements upon applied forces and torques, various calculations must be performed at each simulation step.

First, the forward kinematics module uses the Denavit-Hartenberg (DH) parameters with the current joint angles to calculate homogenous transformation matrices that describe the poses of all leg links with respect to the hip. Second, Jacobian matrices for each link are computed to transform Cartesian forces and torques into the joint parameter space. Third, the dynamics matrices and vectors for (1) are computed and used to determine the movements of the leg joints. It is important to note that this simulator is able to handle forces on each link, because the forward kinematics and the Jacobian matrices are also calculated for each link.

Joint limits are modeled as a unilateral spring damper systems which are optimally damped with respect to overshoot according to the optimal control design research in [10]. In addition, a maximum torque value is given for each joint. If it is exceeded, the wall is deactivated in order to simulate breaking of the respective leg joint.

B. Hand

The hand simulator is based on an existing model of G. Stillfried [11] that consists of 22 revolute joints. The DoF are distributed as shown in Fig. 3(b), which assigns five DoF for both the Thumb and the Pinky finger, and four DoF for the Index, Middle and Ring finger. The colored arrows

TABLE II

THE CONSTANTS USED FOR THE LEG SIMULATOR. THE VALUES WERE TAKEN FROM [2].

Parameter	Component/Joint	Value
Lengths	Thigh	$0.389\,\mathrm{m}$
	Lower Leg	$0.305\,\mathrm{m}$
	Ankle	$0.139\,\mathrm{m}$
	Foot	$0.270\,\mathrm{m}$
Masses	Thigh	$10.340\,\mathrm{kg}$
	Lower Leg	$4.040\,\mathrm{kg}$
	Foot	$1.010\,\mathrm{kg}$
Ranges of Motion	**Hip**	
	Flexion/Extension	$120°/20°$
	Adduction/Abduction	$45°/30°$
	Rotation	$35°/45°$
	Knee	
	Flexion/Extension	$140°/2°$
	Ankle	
	Flexion/Extension	$20°/35°$
	Adduction/Abduction	$15°/10°$
	Rotation	$10°/10°$
Moments of Inertia	**Hip**	
	X	$0.16898\,\mathrm{kg\cdot m^{-2}}$
	Y	$0.17809\,\mathrm{kg\cdot m^{-2}}$
	Z	$0.04646\,\mathrm{kg\cdot m^{-2}}$
	Lower Leg	
	X	$0.06181\,\mathrm{kg\cdot m^{-2}}$
	Y	$0.06271\,\mathrm{kg\cdot m^{-2}}$
	Z	$0.00720\,\mathrm{kg\cdot m^{-2}}$
	Foot	
	X	$0.00087\,\mathrm{kg\cdot m^{-2}}$
	Y	$0.00471\,\mathrm{kg\cdot m^{-2}}$
	Z	$0.00488\,\mathrm{kg\cdot m^{-2}}$
Centers of Gravity	Thigh	$0.1815\,\mathrm{m}$
	Lower Leg	$0.1675\,\mathrm{m}$
	Foot	$0.070\,\mathrm{m}$

indicate the axis of rotation, while the black coordinate axes represent the poses of the links. Again, the Denavit-Hartenberg method was used for calculating the kinematics and the Jacobian matrices. The DH parameters of each finger are listed in Table III.

In comparison to the leg, the hand simulation does not make use of the mass matrix. The reason is in the difference of the forces that originate from the dynamics and those of the space glove. It appears that the resistive forces of the space glove are orders of magnitude greater than the inertial forces to accelerate the finger. To this end, the inertial forces are neglected and the dynamics equation (1) used for simulating the hand motions is substantially simplified, since the acceleration term drops out.

III. SIMULATOR

The STAMAS simulator uses the kinematic and dynamic human limb models that are described in the previous section. To appropriately simulate the functionality of the STAMAS devices, the simulator has some more features. First, it

TABLE III

THE DH-PARAMETERS OF THE HAND MODEL. COURTESY OF G. STILLFRIED.

Finger	$\alpha/(\mathrm{degrees})$	$a/(\mathrm{m})$	$\theta/(\mathrm{degrees})$	$d/(\mathrm{m})$
Thumb	0.00	0.0000	0.00	0.0000
	-90.00	12.4830	-162.29	45.2362
	42.96	11.9745	69.05	-51.4408
	-90.00	0.0000	23.84	79.5515
	12.11	33.9902	0.00	0.0000
Index	0.00	0.0000	0.00	0.0000
	-90.00	0.0000	-30.25	-71.0328
	-31.63	28.7613	59.50	42.2282
	18.57	27.6220	0.00	0.0000
Middle	0.00	0.0000	0.00	0.0000
	90.00	0.0000	173.98	103.2374
	4.34	51.4110	11.96	-110.0265
	16.88	33.3214	0.00	0.0000
Ring	0.00	0.0000	0.00	0.0000
	-90.00	0.0000	22.16	44.6171
	4.71	48.0270	87.45	137.5695
	-10.12	3.6451	0.00	0.0000
Little	0.00	0.0000	0.00	0.0000
	98.22	29.7444	56.13	-22.1891
	-90.00	0.0000	-10.03	86.8373
	15.92	31.4030	41.14	-82.6863
	0.00	24.9804	0.00	0.0000

comprises a device viewer that includes the visualization of forces, torques, and movements that occur during simulation. And second, it contains a module for calculating the interaction forces from the exoskeleton devices. This section sketches these components and the implementation of the simulator in Simulink.

A. Visualization

The visualization is an essential tool that complements the simulator. The goals that were followed while designing the visualization are:

1) The visualization should be able to show the effects of the devices on the astronaut. This means that, when the device is active (i.e., the tendons are helping the user close the hand) one must be able to see the kinematic changes on the astronaut and the amount and direction of forces/torques the device is applying.
2) The visualization should provide an easy to use interface to connect the controller.
3) Safety notifications (e.g., complete stop and color change when torque limits are reached) should be visible and easy to implement.

It is important to note that this visualization is not intended to be a prefect representation of the human body or the devices, but rather should present a simplified geometry to support the clarity of presentation of the important data, i.e., of the force vectors and joint movements. However, visualization models should be accurate enough to provide intuitive views on the limbs.

TABLE IV

LENGTHS AND RANGES OF MOTION USED FOR THE DESIGN AND SIMULATION OF THE HAND SIMULATOR. NOMENCLATURE CAN BE SEEN IN FIG. 3(B).

Parameter	Finger	Phalanx	Value
Lengths	Thumb	MC1	0.0280 m
		PP1	0.0230 m
		PD1	0.0240 m
	Index	PP2	0.0265 m
		PM2	0.0237 m
		PD2	0.0232 m
	Middle	PP3	0.0280 m
		PM3	0.0278 m
		PD3	0.0260 m
	Ring	PP4	0.0276 m
		PM4	0.0256 m
		PD4	0.0229 m
	Little	PP5	0.0251 m
		PM5	0.0192 m
		PD5	0.0196 m
Ranges of Motion	Thumb	CMC1.1	$0.000 \leq \theta \leq 1.285$
		CMC1.2	$-0.762 \leq \theta \leq 0.363$
		MCP1.1	$-0.484 \leq \theta \leq 0.336$
		MCP1.2	$-0.805 \leq \theta \leq 0.829$
		IP1	$-0.482 \leq \theta \leq 1.317$
	Index	MCP2.1	$-0.809 \leq \theta \leq 0.132$
		MCP2.2	$-0.556 \leq \theta \leq 1.152$
		PIP2	$-0.066 \leq \theta \leq 2.048$
		DIP2	$-0.397 \leq \theta \leq 1.366$
	Middle	MCP3.1	$-0.397 \leq \theta \leq 0.152$
		MCP3.2	$-0.599 \leq \theta \leq 1.483$
		PIP3	$-0.126 \leq \theta \leq 2.017$
		DIP3	$-0.412 \leq \theta \leq 1.515$
	Ring	MCP4.1	$-0.407 \leq \theta \leq 0.250$
		MCP4.2	$-0.687 \leq \theta \leq 1.536$
		PIP4	$-0.179 \leq \theta \leq 1.980$
		DIP4	$-0.347 \leq \theta \leq 1.281$
	Little	IMC45	$0.000 \leq \theta \leq 0.503$
		MCP5.1	$-0.714 \leq \theta \leq 0.106$
		MCP5.2	$-0.908 \leq \theta \leq 1.659$
		PIP5	$-0.279 \leq \theta \leq 1.796$
		DIP5	$-0.231 \leq \theta \leq 1.376$

The DLR robot viewer presented in [12] was used as a basis for the STAMAS viewer, as it has the advantageous properties of being easily connectable to Simulink and already supports graphical and numerical visualization of force and torque vectors. Fig. 4 shows how the viewer visualizes the leg and hand. It also shows the force attack point of the bearings and the forces the devices apply on the limbs.

Another important characteristic of the viewer is that it is interactively configurable. The view on the limbs can be shifted and reoriented by the mouse, as it is standard for virtual reality viewers. More remarkable, the leg and the finger can be clicked to change the visualization mode of the forces and torques. The force and torque vectors can either be visualized by straight arrows for the forces and round arrows for the torques, or by numerical displays. These numerical displays have the advantage of precisely showing the force and torque strengths as numbers, while the arrows intuitively show the direction and qualitatively the strength represented by the arrow sizes.

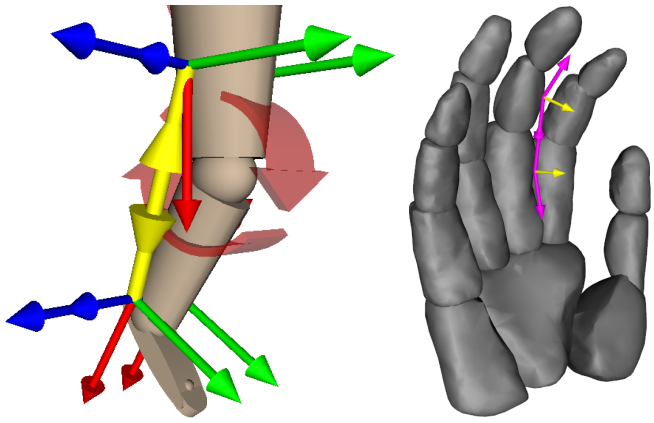

Fig. 4. Visualization of the leg and the hand in the STAMAS Viewer.

B. Force Computation

The actuator forces are transmitted by bearings and fixation points on the device structure to the device. This section concentrates on the hand device, because this is the more complex case with respect to the force transmission. Fig. 4 shows exemplary the actuator forces that are transmitted by a tendon via bearings to the middle finger. It is obvious that the forces at the finger tip can only act in the direction of the tendon. At the other roller bearings, the forces acting on the finger have the direction of the vector sum of forces defined by the tendon in front of and behind each bearing.

After determining the bearing force vectors they are transformed into the joint space. To this end, the forces are first transformed into the coordinate axes of the respective links by using the adjoint matrices that yield from the force attack points [13]. Then the transformed forces are directly transformed into the joint space using the Jacobian matrices. This step yields the joint torques caused by the actuator forces. These torques are then used in the dynamics equation of motion (1) to determine the movements of the device.

C. Implementation Details

The simulator was implemented as a Simulink model. The root level of the Simulink model for the case of the hand device is shown in Fig. 5. The leg model looks very similar. Both models contain the central control unit (CCU) on the left side and the device simulator on the right side. For controlling the real devices, the latter block may just be replaced by the s-function for interfacing with the exoskeletons.

The simulator block contains all above described modules. Their implementation is shown in Fig. 6. The simulation parameters may be adjusted by changing the parameter values in the respective Simulink blocks. Similarly, the values are displayed in Simulink scopes. Both elements form the expert GUI, which is an extremely powerful tool as it provides access to all simulation parameters.

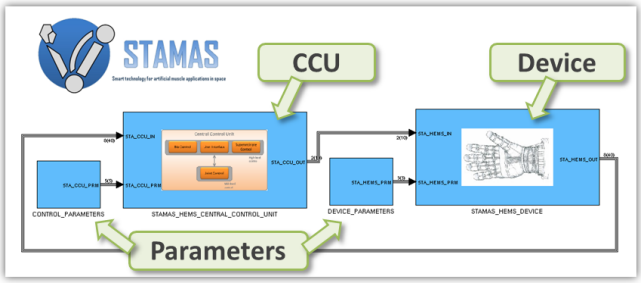

Fig. 5. The root level of the Simulink Computer Software Unit (CSU) exemplarily shown for the hand demonstrator (HEMS).

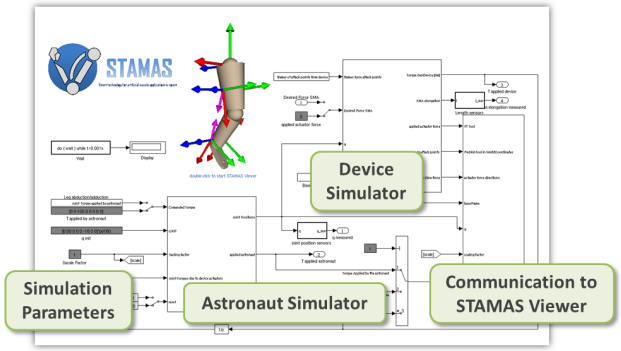

Fig. 6. The simulator subsystem contains the modules for calculation the kinematics and dynamics of the astronaut's limb and of the device.

IV. Simulation Results

Simulations have been conducted for both demonstrators. They shall show that the ranges of movements are sufficient for the planned tasks and determine the required actuator forces.

The methodology was as follows. The Simulink model was initialized with predefined initial parameters and conditions. Then, the model was started and it ran without changing the parameters until a steady state condition was reached. Finally, external forces were applied and the simulation data was acquired and saved into workspace variables. The recorded variables were actuator forces, joint angles and torques applied by the astronaut, the device and for the hand model the resulting torque due to EVA glove stiffness and air pressure.

A. Leg

For the leg device simulation, the initial elastic band length has been set to $0.50\,\mathrm{m}$ and the leg joint angles to the relaxed configuration, i.e., in $[0, 0, 0, 0, 0, 0, -18, 0]\,\mathrm{deg}$. The joint stiffnesses have been set to $[15, 15, 15, 9.5, 11, 15, 15, 15]\,\mathrm{Nm/rad}$ and the damping values to 6% of the critical damping. Two different types of simulations were conducted. For the first one, a configuration was chosen to simulate the effects of the gravitational forces (that would occur on earth) and the increase in torques as the astronaut extends his leg. A second simulation was conducted to determine the effects on the knee joint for different exercising levels while walking.

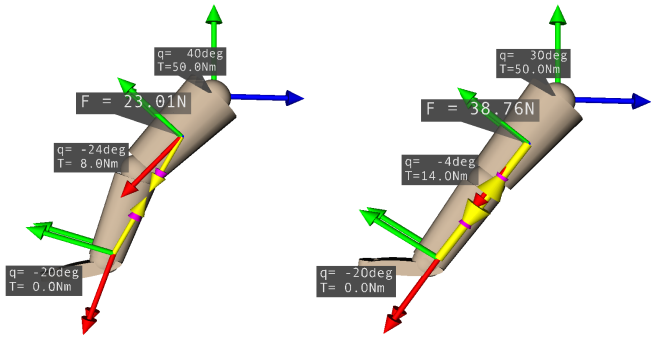

Fig. 7. As the human applies a higher torque, the knee angle increases (the leg stretches) and with it the torque produced by the exercising device. Two different positions are shown. In the left figure, the leg is approximately 50% of the full extension, and on the right, the leg is almost fully extended. Thus, the applied force by the device is about half of the force for the left pose, and reaches the complete commanded force for the right one.

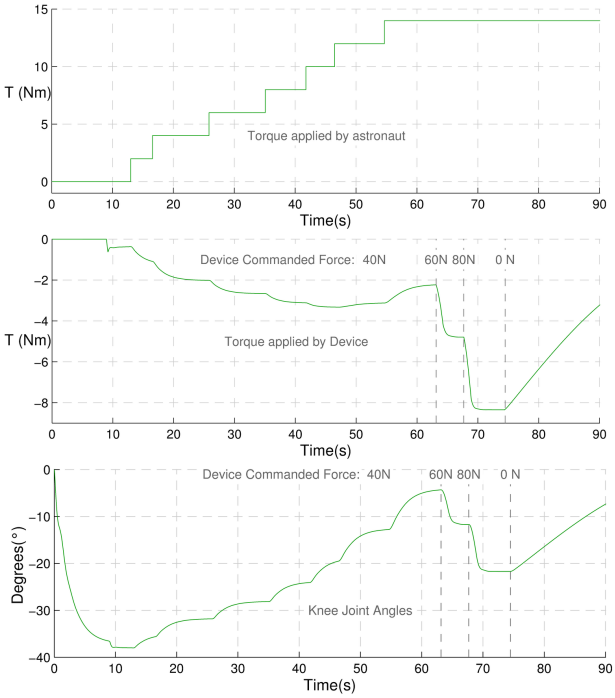

Fig. 8. The graphs above show the evolution of the torques and joint angles during the first simulation. It can be clearly seen that as the human increases the knee joint torque, the angle increases and the device applies a higher compression force, thus increasing the torque in the joint. Once the commanded force is increased, the device applies a higher torque on the knee joint producing an angle decrease. Finally, the actuators need a certain time to cool down and to return to their original form, which can be seen in the final section of the plots.

For the first simulation, a torque of $50\,\mathrm{Nm}$ was applied on the hip joint (third DoF, i.e., flexion/extension). The steady state for this configuration is $[0, 0, 47, -38, 0, -27, 0, 0]\,\mathrm{deg}$. The device is then turned on and the first exercise level is activated. This corresponds to an actuator force of $40\,\mathrm{N}$. Then the commanded compression force of the elastic band is increased to $60\,\mathrm{N}$ and then to $80\,\mathrm{N}$. Finally, the device is turned off and it is possible to see how the SMA actuators start to cool down and gradually decrease the applied force. The human applied torques go from 0 to $14\,\mathrm{Nm}$. Fig. 7 shows two stages during the leg extension. It is possible to see that

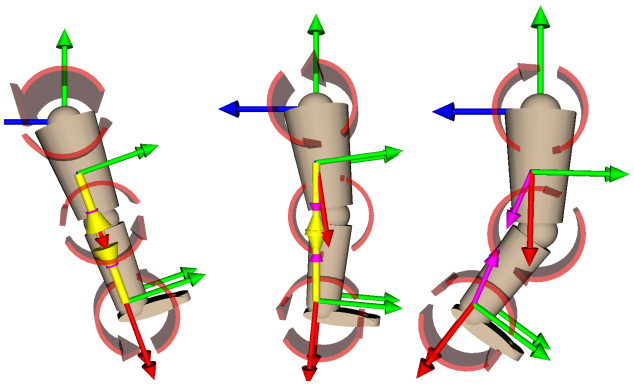

Fig. 9. Three stances while walking with the leg device.

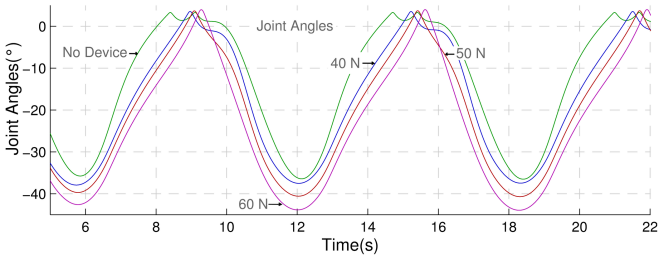

Fig. 10. The graph shows the evolution of knee joint angles while the subject walks. The successive lines represent various device configurations: no active device, and forces of 40 N, 50 N and 60 N.

the force applied by the device becomes higher if the leg extends, as shown in Fig. 8.

For the second simulation, the astronaut leg simulator is started and joints are commanded an oscillating pattern similar to the one joints would perform while walking. The goal is to reach the three basic stances associated with walking, shown in Fig. 9. Once the model is "walking", the exercising level is consecutively increased from one to three, resulting in actuator forces of 40 N, 50 N and 60 N. The exercise levels were chosen to increase the resistance for walking by a factor of 2, 2.5 and 3.

Fig. 10 shows the evolution of the knee joint angle while the subject is "walking" in four different training conditions: green - the device is turned off; blue - the device applies a force of 40 N; red - the device applies a force of 50 N; and magenta – the device applies a force of 60 N. The curves exhibit a relative displacement in the x-axis depending on the actuator force. This shows that as the exercise level increases the astronaut is impelled to apply higher torque to the knee joint to reach the same position.

B. Hand

The hand simulation was mainly designed to determine the actuators force needed to close the astronaut hand while wearing an EVA suit fully pressurized including the effects of the thermal micrometeoroid garment (TMG). As the results are similar for each finger, this section only presents the simulation for the middle finger.

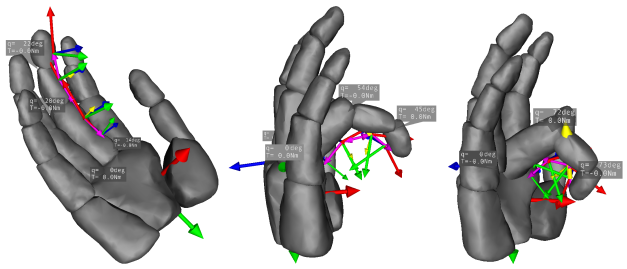

Fig. 11. The force applied on the tendon is increased until the hand is fully closed. Due to the increase of stiffness and decrease of applied torque in the MIP joint full closure is not possible to achieve, unless the human applies an extra torque in some of the joints.

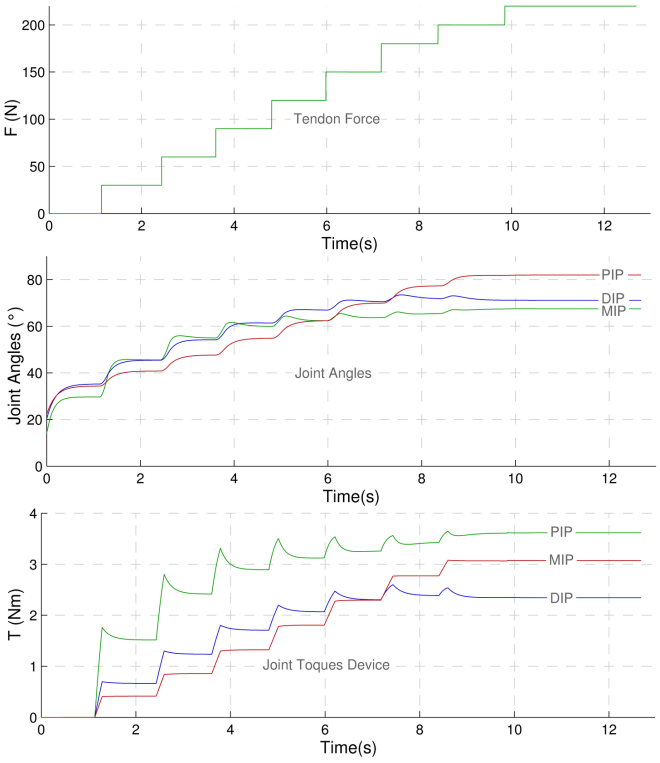

Fig. 12. The graphs above show the results of the first hand simulation. It is possible to see that there is a point where even though the force is increase the joint angles will not increase and for the case of the PIP angle it will decrease. This effect is due to the increase of torque due to stiffness of the EVA and the mechanical configuration of the system.

TABLE V

THE APPROXIMATE VALUES OF THE STIFFNESS AND DAMPING ADDED BY THE GLOVE EFFECTS. THE VALUES WERE ADAPTED FROM FAVETTO [14].

Joint	Stiffness Coefficient / (Nm/rad)	Damping Coefficient / (Nm/(s rad))
MCP1	6.4	1
MCP2	5.2	1
PIP	3.2	1
DIP	2.8	1

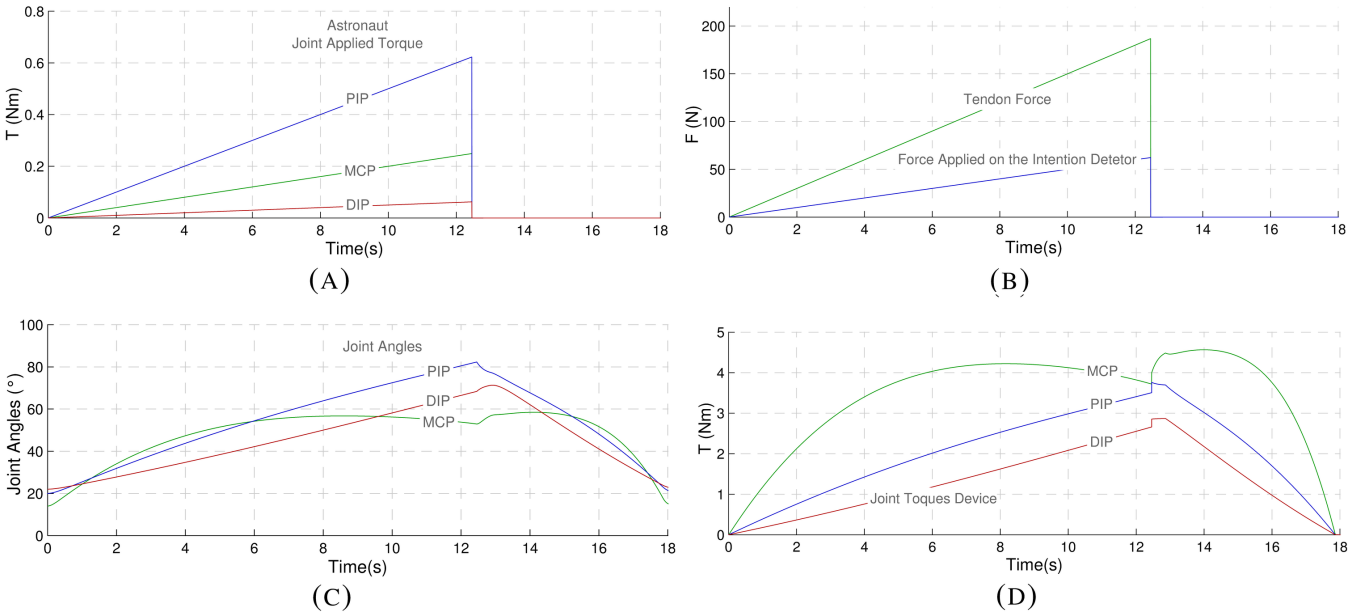

Fig. 13. The graphs above show the results of the second hand simulation.

The initial conditions of the hand simulator are: The user applies a small torque in the joints $[0, 1.5, 1, 0.8]\,\mathrm{Nm}$, and the effects of the EVA glove are active. The stiffness and damping values are detailed in Table V, and the joint angles correspond to relaxed hand position, i.e., $[0, 14, 20, 20]\,\mathrm{deg}$. Fig. 11 shows the hand at three different instants during simulation.

For a tendon force of $180\,\mathrm{N}$, the hand is nearly completely closed. Note that a further increase in the force does not lead to a further change of position, because of the given distance of the bearings to the finger. In principle, however, the astronaut could further close his fingers, if he/she would apply high finger torques that exceed the resistance of the glove.

A second simulation was conducted to see the effects of progressive increase in force. It simulates the force pattern the user would apply on the finger tips that are then amplified by the controller to close the glove (a force feedforward control approach is used [15], [16]). The selected feed forward gain is 3. The simulation also exposes the resulting configuration, if at any given time that force is diminished or stopped.

Fig. 13 shows the torques applied by the astronaut at the different finger joints. The applied torques at the MCP and the PIP joint are not amplified, as they represent the initial torques in the simulation. The torque at the DIP joint, T, results from the force that the astronaut would apply on the force sensor in the finger tip and would be then amplified by the controller. As the astronaut closes the hand, the resistive force of the glove increases and the astronaut must apply higher torques to keep closing the hand. In the second part of the simulation, the astronaut stops pushing against the tip sensor and the actuators start to cool down. The air pressure causes the glove to open the hand.

V. Conclusions

The interactive STAMAS simulator includes an astronaut leg and its corresponding semi-passive exercising device, an astronaut hand and the EVA exoskeleton device, the device kinematics with the force attack points and simulation of the air pressure and bulk stiffness of the EVA glove. The simulator further comprehends virtual reality visualization for the hand and leg based on the DLR robot viewer [12].

The STAMAS simulator is designed to accurately simulate the astronaut limb movements and behavior during the different device configurations. In order to validate the device concepts with respect to movement and force ranges, a series of simulations was carried out. The results of the simulations reveal that the planned device configurations are feasible. The desired movements can be covered by the conceptual kinematic structure. With regard to the forces, the simulations determined forces of up to $180\,\mathrm{N}$ for the hand exoskeleton and $150\,\mathrm{N}$ for the leg exercising device, which would be needed for perfectly executing the planned tasks. However, even if only a fraction of these ideal force values are reached, the devices would offer a huge benefit for the astronauts.

The simulator, as implemented in Simulink, may be adapted easily to elegantly take into account future design changes of the device concepts and conduct meaningful simulations accordingly. Its implementation in Simulink has a further major advantage, as it turns the simulator into a test environment for the STAMAS controllers, which are also implemented in Simulink. To this end, the controller may be tested on the simulation environment, before running on the real systems. Hence, hardware stress may be reduced and possible damage of the device prototypes and its human operator averted.

REFERENCES

[1] M. Collado, "Publishable summary, deliverable no.: D7.11," Dec. 2014, European Project STAMAS FP7-SPACE-312815. [Online]. Available: www.stamas.eu

[2] J. M. Christensen, J. W. McBarron, J. T. McConville, W. R. Pogue, R. C. Williges, and W. E. Woodson, *Man-systems integration standards NASA-STD-3000*. National Aeronautics and Space Administration (NASA), Jul. 1995, vol. 1, revision B.

[3] J. Denavit and R. S. Hartenberg, "A kinematic notation for lower-pair mechanisms based on matrices," *ASME Journal of Applied Mechanics*, vol. 22, pp. 215–221, 1955.

[4] H. Asada and S. J.-J. E., *Robot Analysis and Control*. John Wiley, 1986.

[5] J. J. Craig, *Introduction to Robotics Mechanics and Control*, 2nd ed. Addison-Wesley Publishing Company, Inc., USA, 1989.

[6] C. A. Evans, J. A. Robinson, J. Tate-Brown, T. Thumm, J. Crespo-Richey, D. Baumann, and J. Rhatigan, "International space station science research accomplishments during the assembly years: An analysis of results from 2000–2008," Jul. 2009, Technical Report TP-2009-213146.

[7] H. Gray, *Anatomy of the human body*. Lea & Febiger, 1918.

[8] N. Costa and D. G. Caldwell, "Control of a biomimetic "soft-actuated" 10dof lower body exoskeleton," in *IEEE/RAS-EMBS Int. Conf. on Biomedical Robotics and Biomechatronics (BioRob)*. IEEE, 2006, pp. 495–501.

[9] H.-J. Chung, "Optimization-based dynamic prediction of 3d human running," Ph.D. dissertation, University of Iowa, 2009.

[10] T. Hulin, R. González Camarero, and A. Albu-Schäffer, "Optimal control for haptic rendering: Fast energy dissipation and minimum overshoot," in *IEEE/RSJ Int. Conf. on Intelligent Robots and Systems (IROS)*, Tokyo, Japan, Nov. 2013, pp. 4505–4511.

[11] G. Stillfried, U. Hillenbrand, M. Settles, and P. van der Smagt, "MRI-based skeletal hand movement model," in *The Human Hand as an Inspiration for Robot Hand Development*. Springer, 2014, pp. 49–75.

[12] T. Hulin, K. Hertkorn, and C. Preusche, "Interactive features for robot viewers," in *Int. Conf. on Intelligent Robotics and Applications (ICIRA)*, Montreal, Canada, Oct. 2012, pp. 181–193.

[13] R. M. Murray, Z. Li, and S. S. Sastry, *A mathematical introduction to robotic manipulation*. CRC press, 1994.

[14] A. Favetto, "Glove exoskeleton for extra-vehicular activities," Ph.D. dissertation, Politecnico di Torino, Italy, 2014.

[15] J. J. Gil and E. Sánchez, "Control algorithms for haptic interaction and modifying the dynamical behavior of the interface," in *Int. Conf. on Enactive Interfaces*, Genoa, Italy, Nov. 2005.

[16] T. Hulin, C. Alessandro, B. Vodermayer, and R. Riener, "Evaluation of force feedforward control for actuators with limited dynamics and time delay," in *STAMAS Workshop – Smart technology for artificial muscle applications in space*, Oct. 2015.